

Lasing in electrodeposited ZnO inverse opal

L. K. Teh^{a)} and C. C. Wong

School of Materials Science and Engineering, Nanyang Technological University, Nanyang Avenue, Singapore 639798, Singapore

H. Y. Yang, S. P. Lau, and S. F. Yu

School of Electrical and Electronic Engineering, Nanyang Technological University, Nanyang Avenue, Singapore 639798, Singapore

(Received 31 August 2007; accepted 2 October 2007; published online 19 October 2007)

We report room-temperature ultraviolet lasing in ZnO inverse opals fabricated via colloidal templating with electrochemical infiltration. Lasing occurs above an excitation threshold of 0.38 MW/cm^2 . Lasing modes associated with radiative recombinations of exciton-exciton (ex-ex) and electron-hole plasma (EHP) were discerned. Compared to ZnO polycrystalline film, lasing wavelength blueshifts and ex-ex lasing with a narrower bandwidth have been realized. Tuning the primary photonic pseudogap of inverse opals to gain maximum reduces the threshold for EHP lasing. We infer that periodic structures facilitate strain-induced change in lasing energy and provide modulation in refractive index for enhanced light confinement as well as optical feedback. © 2007 American Institute of Physics. [DOI: 10.1063/1.2801358]

The optical feedback mechanisms in nonepitaxial films of semiconductor materials include closed-loop random laser cavity formed by strong optical scattering in a highly disordered polycrystalline thin film and photonic band gap (PBG) light reflector based on Bragg scattering in a photonic crystal (PhC). Typically, random lasing has higher threshold than photonic lasing.¹ The gain enhancement in a PhC can be attained by (1) localization of light over a defect within the PBG whereby it serves as an ultrasmall high-quality microcavity² or (2) reduction in the group velocity of light at a photonic band edge and flatband region which increases the interaction time between light and gain medium for enhanced distributed feedback (DFB).³ Infrared (IR) PhC lasers have been demonstrated in two-dimensional (2D) PhCs, with either defect⁴ or DFB modes.⁵ Enhanced emission in the blue/green wavelengths has also been reported in a 2D PhC based on III-nitride materials⁶ while ultraviolet (UV) lasing has been achieved in a 2D ZnO PhC.⁷ A three-dimensional (3D) PhC with an omnidirectional PBG is essential for complete confinement of light. While modification of emission from semiconductor nanocrystals (NCs) by PBG engineering^{8–10} has been demonstrated in NC-infiltrated 3D opaline PhCs in the visible wavelengths, reports on 3D semiconductor PhC lasers have been scarce. The short wavelength implies a nanometer-scale periodicity which imposes great fabrication challenges. Recently, room-temperature UV lasing has been demonstrated in the flat, high-order bands of 3D ZnO inverse opals fabricated by atomic layer deposition.¹¹ This scheme allows fabrication of PhCs with relatively large lattice constants, which leads to a relaxation of the stringent fabrication requirements. Structural defects inevitably present in these structures introduce disorder that leads to strong scattering and random lasing; hence these devices are labeled as partially ordered random lasers. Later, it has been reported that tuning the first Γ -L pseudogap to gain spectrum can lead to a fivefold reduction in lasing threshold due to enhanced light confinement.¹² However, the

lasing threshold remains high ($>100 \text{ MW/cm}^2$). In this report, we show, by means of electrodeposition infiltration, a high quality 3D ZnO inverse opal, from which room-temperature UV lasing is achieved at a pumping threshold of $\sim 0.38 \text{ MW/cm}^2$, among the lowest in polycrystalline ZnO films.^{11–14} We have further examined the reduction of the lasing threshold through PBG engineering. Since random lasing can also be observed from ZnO polycrystalline thin films, we also compare the lasing spectra between the inverse opal and the unstructured polycrystalline film. We then discuss the role of the periodic structure in improving the lasing characteristics.

ZnO films were deposited on an indium tin oxide coated glass substrate by aqueous-based electrodeposition, which offers several advantages over gas-phase deposition techniques.¹⁵ To obtain ZnO inverse opal, ZnO material was infiltrated into a polystyrene (PS) opaline template, which was subsequently removed by heat treatment. The lattice constant of the inverse opal is a function of the PS sphere diameter for the opaline template. Details of the fabrication have been described elsewhere.¹⁶ A top-view field emission scanning electron micrograph (FESEM) of a ZnO inverse opal is shown in Fig. 1(a). The air spheres are well ordered in

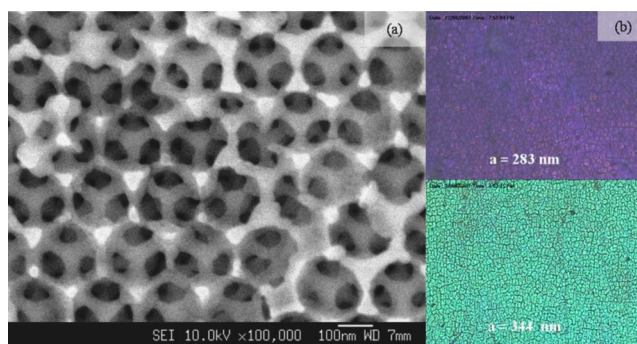


FIG. 1. (Color online) (a) Top-view FESEM of a ZnO inverse opal with lattice constant $a=283 \text{ nm}$. (b) Optical microscope images (magnification of $5\times$) of ZnO inverse opals with lattice constants $a=283 \text{ nm}$ (violet) and $a=344 \text{ nm}$ (green).

^{a)}Electronic mail: laykuan@pmail.ntu.edu.sg

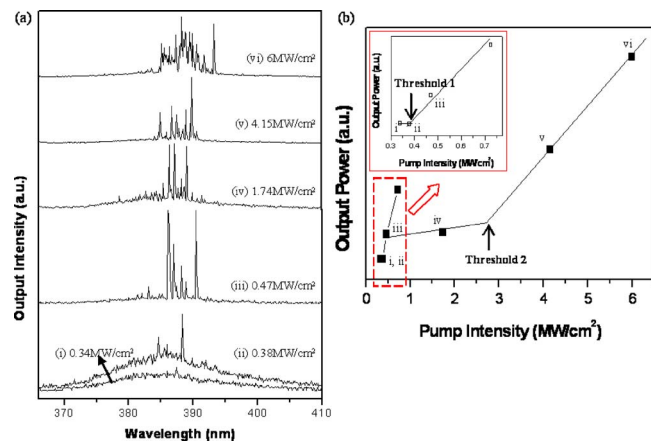


FIG. 2. (Color online) (a) Emission spectra as a function of pump intensity and (b) L - L curve of ZnO inverse opal with $a=283$ nm for increasing pump intensity. Inset: Enlarged view of the L - L curve for low pump intensity region (<1 MW/cm²). The first and second thresholds occur at 0.38 and 2.7 MW/cm², respectively.

a close-packed structure with uniform sphere diameter replicating the opal template. Inside each sphere, the three dark holes correspond to the air spheres at the underlying layer. This reveals the interconnecting nature of the ZnO shells, forming a solid frame. The inverse opal displays iridescent colors corresponding to its primary pseudogap [see Fig. 1(b)]. To overlap the position of the primary pseudogap of the inverse opal with the ZnO gain spectrum, the lattice constant was altered from $a=283$ to 344 nm. The position of the pseudogap was determined by performing optical reflection measurements at normal incidence.

In this study, the ZnO inverse opal exhibits both excitonic (ex-ex) and electron-hole plasma (EHP) laser emissions. The sample was excited at room temperature by a frequency tripled (355 nm) Nd:yttrium aluminum garnet laser at pulsed operation [6 ns full width at half maximum (FWHM), 10 Hz]. The pump stripe of length ~ 1 mm and width ~ 60 μ m was focused onto the ZnO inverse opal by a cylindrical lens and light was illuminated normal to the surface of the sample. Figure 2(a) shows the evolution of the emission spectra with pump intensity. At low excitation intensity, the emission spectrum consists of a single broad spontaneous emission peak at ~ 387 nm with FWHM of ~ 15 nm. As the pump intensity increases above a threshold (~ 0.38 MW/cm²), sharp lasing peaks with linewidth <0.1 nm centered at ~ 387 nm (ex-ex collision) emerge. As

the pump stripe is moved across the sample, at pump intensity just above the threshold, these lasing modes appear periodic and well separated in some cases. The exact origin of the periodicity is unclear at this time, which we intend to investigate further. Further increase in pump power increases the number of lasing modes without shifting the center frequency. From the light-light (L - L) curve given in Fig. 2(b), the presence of a “kink” [point “iii” in the inset of Fig. 2(b)] clearly marks the onset of lasing action at a pump threshold above which the output intensity increases rapidly with excitation intensity. The suppression of the broad spontaneous emission background further confirms that high quality lasing modes have occurred in the sample. The quality factor (Q factor) for these lasing modes can be calculated using $Q=\lambda/\delta\lambda$, where $\delta\lambda$ is the width of the emission mode at wavelength λ . A Q factor of ~ 6500 was obtained with essentially zero spontaneous emission background. The quality of the lasing modes in our work is comparable to^{17–20} or better than^{21,22} the previously reported data for epitaxial ZnO films, albeit with a higher threshold. In addition, when the pump intensity exceeds a second threshold (~ 2.7 MW cm⁻²), the intensity of the ex-ex emission saturates while another group of lasing modes centered at ~ 392 nm (EHP recombination) is excited. The FWHM of the entire spectrum is reduced to ~ 5 nm. In this case, the emission intensity increases with the excitation intensity at a rate slower than the ex-ex emission mentioned earlier and its center frequency shifts toward lower energy, characteristics of an EHP emission.²³ The distinct thresholds and dependence of center frequency on pump intensity make it unambiguous to distinguish the different recombination mechanisms in the sample.

We have also observed enhanced light confinement for the ZnO inverse opal when its primary pseudogap approaches the ZnO gain maximum (~ 387 nm). As shown in Fig. 3(a), for inverse structure with $a=283$ nm, Bragg’s reflection peak which corresponds to the opening of the primary pseudogap is shifted toward the ZnO gain maximum. It is apparent that the ex-ex and EHP laser emissions are well resolved under high optical pumping. The single mode EHP emission does not coincide with the gain maximum and lies within the wavelength range of the pseudogap. For inverse structure with $a=344$ nm, when the primary pseudogap is far away from the gain maximum, the lasing spectrum is dominated by the ex-ex emission, where multiple EHP emission lines coexist and merged with it. The entire lasing spectrum

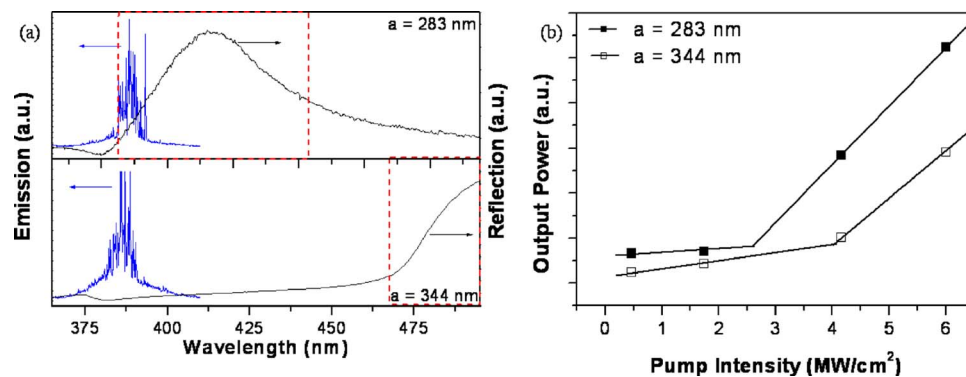


FIG. 3. (Color online) (a) Lasing (pump intensity ~ 6 MW/cm²) and reflection spectra and (b) L - L curves of ZnO inverse opals with different lattice constants. The areas enclosed by dotted lines indicate the position of the primary photonic pseudogap obtained by photonic band structures computed using a freely available software package (Ref. 24).

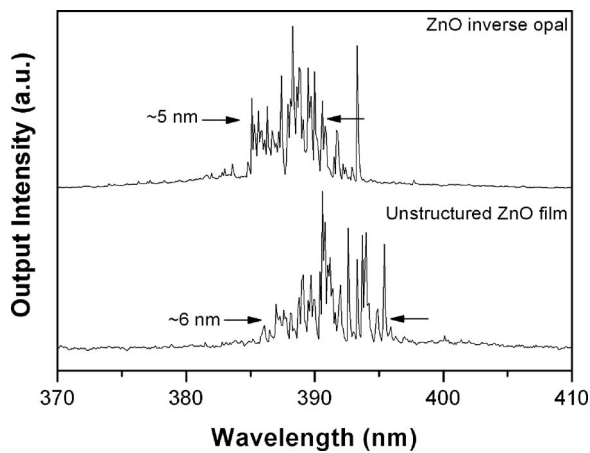


FIG. 4. Lasing spectra under a pump intensity of 6 MW/cm^2 for the electrodeposited ZnO inverse opal and the unstructured ZnO thin film.

is centered at the gain maximum. Figure 3(b) compares the light-light curves for the ZnO inverse opals of different lattice constants. It is evident that the lasing threshold for the EHP emission in ZnO inverse opal has been reduced by half after overlapping the primary pseudogap with the gain spectrum. We attributed the lasing EHP emission for the inverse opal with $a=283 \text{ nm}$ and $a=344 \text{ nm}$ to be photonic lasing and random lasing, respectively. With this, we verified that photonic lasing has a lower threshold than random lasing. It is worth mentioning that the photonic lasing mode changes in frequency with the illumination region on the inverse opal. This suggests that the photonic lasing mode originates from the localized defect mode within the primary pseudogap.

To further evaluate the role of periodic structure on the lasing characteristics, a homogeneous polycrystalline ZnO thin film was deposited and heat treated under the same conditions as a reference sample. The ZnO inverse opal displays ex-ex laser emission lines centered at $\sim 387 \text{ nm}$ while the unstructured ZnO thin film shows EHP laser emission lines centered at $\sim 390 \text{ nm}$ (Fig. 4). This implies improved lasing characteristics in the inverse opal as the ex-ex laser emission can be realized at relatively low pump intensity as compared to the EHP laser emission.²³ Comparison of the lasing spectra between the inverse opal and the unstructured ZnO thin film also reveals a blueshift in lasing energy ($\sim 40 \text{ meV}$) and a narrower bandwidth in the former (5 vs 6 nm). We postulate this to be a consequence of strain-induced shift in the excitonic energy. We performed x-ray diffraction measurements (data not shown) to obtain the lattice parameters of ZnO crystal. From the (101) diffraction peak, the c -axis lattice parameter for the reference film and inverse opal was determined to be approximately 5.196 and 5.202 nm, respectively. The strain along the c axis of the films perpendicular to the substrate is defined by $\varepsilon_{zz}=(c-c_0)/c_0$, where c_0 ($\sim 0.5205 \text{ nm}$) is the lattice parameter in the unstrained crystal. ε_{zz} for the reference film and inverse opal are estimated to be -0.17% and -0.06% , respectively. Both samples are under compressive strain, the inverse opal being less compressive. It has been reported that the excitonic energy of strained ZnO shifts to higher energy as ε_{zz} increases, from

compressive to tensile.²⁵ This is consistent with our results and the magnitude of the change in the excitonic energy is comparable.

In summary, we have achieved room-temperature UV lasing in a 3D ZnO inverse opal fabricated by electrodeposition. There is a blueshift in the stimulated emission with reduced bandwidth in comparison with an unstructured ZnO thin film. The optical gain is further enhanced by localized defect modes within the primary photonic pseudogap, which leads to a twofold reduction in lasing threshold. We deduce that the periodic photonic structure plays a dual role: (1) to induce strain and a change in lasing energy and (2) to provide modulation in refractive index for enhanced light confinement as well as optical feedback.

The authors (L.K.T. and H.Y.Y.) acknowledge the support of Singapore Millennium Foundation Fellowships.

- ¹M. N. Shkunov, M. C. DeLong, M. E. Raikh, Z. V. Vardeny, A. A. Zakhidov, and R. H. Baughman, *Synth. Met.* **116**, 485 (2001).
- ²S. John, *Phys. Rev. Lett.* **58**, 2486 (1987).
- ³J. P. Dowling, M. Scalora, M. J. Bloemer, and C. M. Bowen, *J. Appl. Phys.* **75**, 1896 (1994).
- ⁴O. Painter, R. K. Lee, A. Scherer, A. Yariv, J. D. O'Brien, P. D. Dapkus, and I. Kim, *Science* **284**, 1819 (1999).
- ⁵M. Imada, S. Noda, A. Chutinan, T. Tokuda, M. Murata, and G. Sasaki, *Appl. Phys. Lett.* **75**, 316 (1999).
- ⁶T. N. Oder, J. Shakya, J. Y. Lin, and H. X. Jiang, *Appl. Phys. Lett.* **83**, 1231 (2003).
- ⁷X. Wu, A. Yamilov, X. Liu, S. Li, V. P. Dravid, R. P. H. Chang, and H. Cao, *Appl. Phys. Lett.* **85**, 3657 (2004).
- ⁸P. Lodahl, L. F. van Driel, I. S. Nikolaev, A. Irman, K. Overgaag, D. Vanmaekelbergh, and W. L. Vos, *Nature (London)* **430**, 654 (2004).
- ⁹S. G. Romanov, D. N. Chigrin, C. M. Sotomayor Torres, N. Gaponik, A. Eychmuller, and A. L. Rogach, *Phys. Rev. E* **69**, 046606 (2004).
- ¹⁰Yu. C. Vlasov, K. Luterova, I. Pelant, B. Hönerlage, and V. N. Astratov, *Appl. Phys. Lett.* **71**, 1616 (1997).
- ¹¹M. Scharrer, A. Yamilov, X. Wu, H. Cao, and R. P. H. Chang, *Appl. Phys. Lett.* **88**, 201103 (2006).
- ¹²M. Scharrer, X. Wu, A. Yamilov, H. Cao, and R. P. H. Chang, presented at the *Frontiers in Optics*, Rochester, NY, 2006 (unpublished).
- ¹³H. Cao, Y. G. Zhao, H. C. Ong, S. T. Ho, J. Y. Dai, J. Y. Wu, and R. P. H. Chang, *Appl. Phys. Lett.* **73**, 3656 (1998).
- ¹⁴T. W. Kim, T. Kawazoe, S. Yamazaki, and M. Ohtsu, *Appl. Phys. A: Mater. Sci. Process.* **80**, 1049 (2005).
- ¹⁵D. Lincot, *Thin Solid Films* **487**, 40 (2005).
- ¹⁶L. K. Teh, K. H. Yeo, and C. C. Wong, *Appl. Phys. Lett.* **89**, 051105 (2006).
- ¹⁷D. M. Bagnall, Y. F. Chen, Z. Zhu, T. Yao, S. Koyama, M. Y. Shen, and T. Goto, *Appl. Phys. Lett.* **70**, 2230 (1997).
- ¹⁸Y. Chen, N. T. Tuan, Y. Segawa, H.-J. Ko, S.-K. Hong, and T. Yao, *Appl. Phys. Lett.* **78**, 1469 (2001).
- ¹⁹S. F. Yu, C. Yuen, S. P. Lau, and H. W. Lee, *Appl. Phys. Lett.* **84**, 3244 (2004).
- ²⁰S. P. Lau, H. Y. Yang, S. F. Yu, H. D. Li, M. Tanemura, T. Okita, H. Hatano, and H. H. Hng, *Appl. Phys. Lett.* **87**, 013104 (2005).
- ²¹Z. K. Tang, G. K. L. Wong, P. Yu, M. Kawasaki, A. Ohtomo, H. Koinuma, and Y. Segawa, *Appl. Phys. Lett.* **72**, 3270 (1998).
- ²²X. Q. Zhang, I. Suemune, H. Kumano, Z. G. Yao, and S. H. Huang, *J. Lumin.* **122-123**, 828 (2007).
- ²³Z. K. Tang, M. Kawasaki, A. Ohtomo, H. Koinuma, and Y. Segawa, *J. Cryst. Growth* **287**, 169 (2006).
- ²⁴S. G. Johnson and J. D. Joannopoulos, *Opt. Express* **8**, 173 (2001).
- ²⁵T. Makino, T. Yasuda, Y. Segawa, A. Ohtomo, K. Tamura, M. Kawasaki, and H. Koinuma, *Appl. Phys. Lett.* **79**, 1282 (2001).